Measuring the Frequency Response of Gigabit Chip Photodiodes

Paul D. Hale, *Member, IEEE*, Tracy S. Clement, *Member, IEEE*, Dylan F. Williams, *Senior Member, IEEE*, Elyas Balta, and Narayan D. Taneja

***Abstract*—We describe a calibration and measurement procedure for determining the intrinsic frequency response of gigabit chip photodiodes embedded in simple test fixtures. The procedure is unique because we make the measurements in the time domain using a calibrated oscilloscope, and we then apply frequency-domain mismatch corrections to remove the effects of the fixture, bias T, and cables from the measurements. We demonstrate the procedure on photodiodes with an active region of approximately 150-μm diameter excited by short 800-nm wavelength optical pulses.**

***Index Terms*—Equivalent circuits, frequency response, measurement, photodetectors, photodiodes.**

I. Introduction

We developed a procedure for rigorous calibration and measurement that determines the frequency response of chip photodiodes embedded in simple test fixtures. Such photodiodes are commonly used in applications such as gigabit Ethernet and Fibre Channel. In our measurement, we excite the photodiode with an optical impulse source and measure the combined impulse response of the photodiode, test fixture, and cable assembly (bias T, cable, and adapters) using a calibrated oscilloscope. We then convert the measured impulse response into the frequency domain and de-embed the response of the fixture and cable assembly with rigorous microwave methods. This allows us to fully calibrate the measurements and to directly determine the photodiode's intrinsic frequency response.

II. Experimental Configuration and Oscilloscope Calibration

Fig. 1 shows our experimental configuration. We used a mode-locked, Ti : sapphire laser which provided pulses with full-width at half-maximum (FWHM) of less than 100 fs at a wavelength of 800 nm and a repetition rate of approximately 80 MHz. We split the laser beam to simultaneously provide an optical pulse to the detector under test in one arm and a trigger signal for the oscilloscope in the other arm. The sample arm contained a 2-m length of single-mode fiber, with the output coupled into a gradient-index lens, which focused the light from the fiber onto the detector under test. The photodiode was designed to block light falling outside its active region. Dispersion in the optical fiber broadened the optical pulse to about 4 ps FWHM, which was negligible compared to the response times of our chip photodiodes. The optical system was designed to make optical reflections between the photodiode, lenses, and fiber negligible.

We calibrated the phase response of our sampling oscilloscope, which has a 50-GHz bandwidth, with the "nose-to-nose" calibration procedure [1]–[4]. The calibration included corrections for time–base distortion [5], impedance mismatch [4], [6], time–base drift [7], and time–base jitter [8]. We calibrated the magnitude response of our oscilloscope by direct comparison to a calibrated power meter [4], [6].

We normalized the resulting oscilloscope calibration so that the oscilloscope measures V_c, the voltage that a source with a 50-Ω impedance would deliver to a matched 50-Ω load. Thus, while V_c has been corrected for the frequency response and time–base errors of the oscilloscope, it has not been corrected for the impedance mismatch of an arbitrary source. This further correction will be discussed in Section IV. The oscilloscope calibrations are band-limited, so V_c is a frequency-domain quantity.

We connected the photodiode, test fixture, and cable assembly sketched in Fig. 1 to our sampling oscilloscope and measured the response of the entire system to the optical pulses over a time period of 10 ns, just under the repetition period of our laser. Fig. 2 shows the measured waveform after averaging and correcting for time–base distortion [5]. Since the optical pulses are extremely short, we can reasonably assume that the measured waveform is that of the convolved impulse responses of the photodiode, test fixture, and cable assembly. The measured waveform also includes multiple reflections between the oscilloscope, cable assembly, photodiode test fixture, and the photodiode itself. The solid curve in Fig. 3 shows the Fourier transform of the pulse shown in Fig. 2 with correction for the oscilloscope's frequency-domain response. The small ripple (roughness) in the frequency-domain data is due to the multiple reflections.

III. Characterization of Cable Assembly and Test Fixture

Fig. 4(a) shows the fixture we used to test the photodiodes. The fixture consisted of an inexpensive printed circuit board through-type male SMA mount. The photodiode chip was fastened to a metal block with conducting epoxy, and the block was bolted to the electrical ground of the SMA mount. We bonded a gold wire to the photodiode's anode contact pad and epoxied

Manuscript received March 28, 2001; revised June 8, 2001.

P. D. Hale, T. S. Clement, and D. F. Williams are with the National Institute of Standards and Technology, Boulder, CO 80303 USA (e-mail: hale@boulder.nist.gov).

E. Balta was with UDT Sensors, Inc., Hawthorn, CA 90250 USA. He is now with Integrated Micromachines, Monrovia, CA 91016 USA.

N. D. Taneja is with UDT Sensors, Inc., Hawthorn, CA 90250 USA.

Publisher Item Identifier S 0733-8724(01)07896-3.

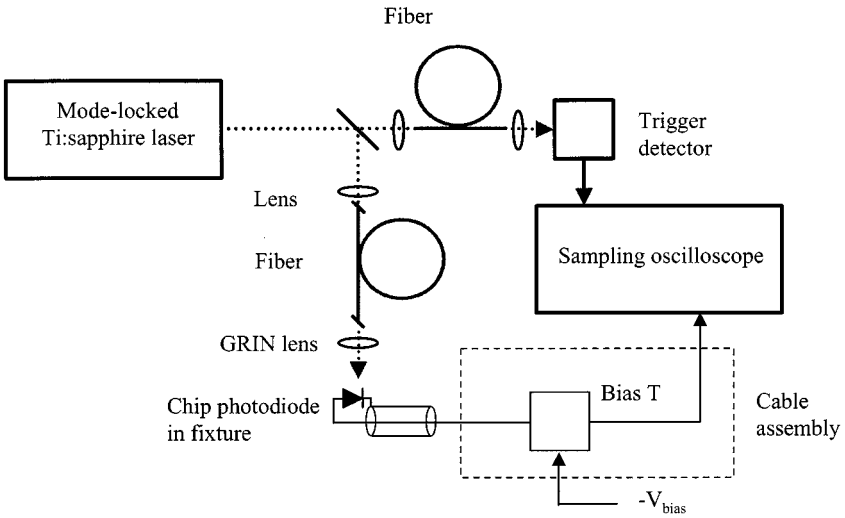

Fig. 1. Simplified schematic of the time-domain measurement system. The fiber has angled ends and the lenses have antireflection coatings to eliminate multiple optical pulses.

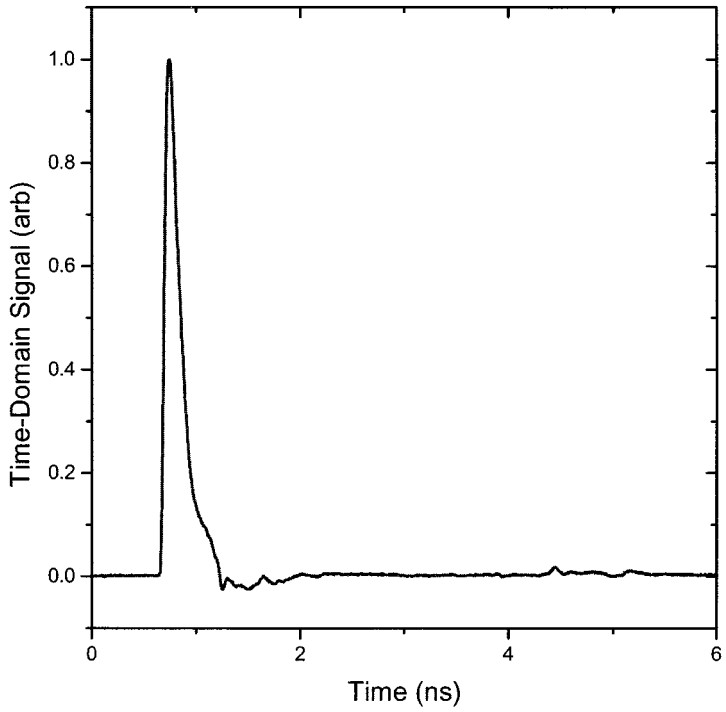

Fig. 2. Typical measured time-domain waveform after averaging and corrections for time–base distortion. Only the first 6 ns of the 10-ns recorded waveform is shown.

the other end of the wire to the center conductor of the SMA mount.

We used a frequency-domain vector network analyzer to measure the scattering parameters S_{ij}^{C} of the cable assembly directly. However, we were unable to measure the two-port scattering parameters of the test fixture in which we mounted the photodiodes, since we were unable to form direct electrical connections to the terminals. To circumvent this problem, we developed a simple electrical model of the test fixture from measurements of reflections at its single coaxial port.

Fig. 4(b) shows the electrical model we developed for the test fixture. To determine the model elements we fabricated open-circuited and short-circuited fixtures with no embedded photodiodes, and measured their reflection coefficients at frequencies up to 6 GHz. The short-circuited fixture had a bonding wire between the photodiode mounting block and the SMA center conductor. The open-circuited fixture had no wire bond at all.

We found the length of the 50-Ω coaxial transmission line of the model of Fig. 4(b) from the phase of the measured reflection coefficient of the open-circuited fixture. We modeled the internal impedance Z_i of the bonding wire as that of a cylindrical wire with finite conductivity, using the analytic expression [9]

$$Z_i = \frac{-TJ_0(Tr_0)}{2\pi r_0 \sigma J_0'(Tr_0)} \tag{1}$$

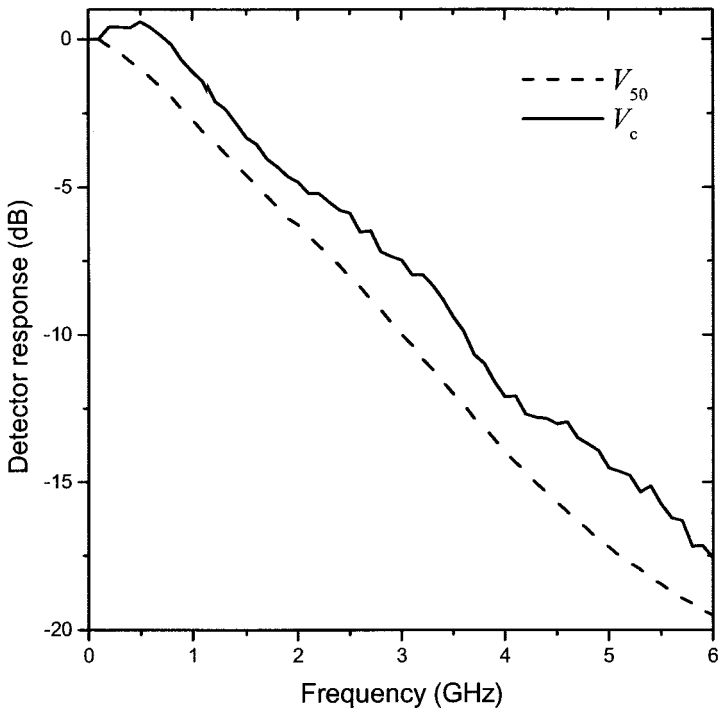

Fig. 3. Frequency response of the photodiode. The solid curve is V_c and the dashed curve is V_{50}, the response with the correction described in (4). The curves are normalized to 0 dB at 100 MHz.

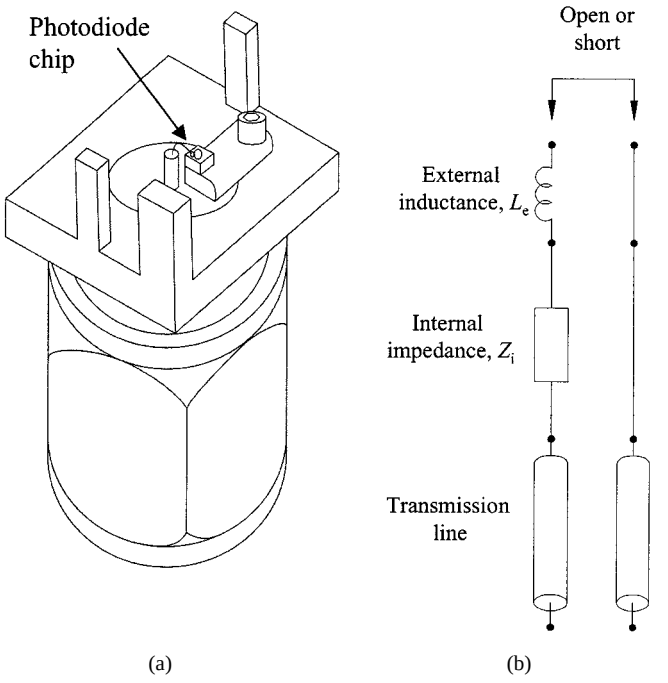

Fig. 4. (a) Sketch of our coaxial test fixture. (b) Electrical model of the test fixture with standard terminations.

where r_0 is the wire radius, σ is the bulk conductivity ($3.28 \times 10^7\ \Omega^{-1} \cdot \mathrm{m}^{-1}$) of the bond wire, $T^2 = i\omega\mu_0\sigma$, μ_0 is the permeability of free space, ω is the frequency in radians, and $J_0(x)$ and $J_0'(x)$ re zeroth-order Bessel function and the Bessel function's derivative, respectively. We adjusted the radius and length of this wire to best match the loss of the short-circuited fixture. Finally, we adjusted the external inductance L_e of the wire to match the phase of the reflection coefficient of the short-circuited fixture. Figs. 5 and 6 compare the measurements to their modeled values.

The resulting model parameters did not agree closely with the values we expected from physical measurements of the coaxial line's length and wire bond's length and diameter. However, we may have overestimated the length of the coaxial line in the model, since we used an open-circuited measurement that included fringing capacitance at the end of the fixture. Also, the conducting epoxy used in constructing the fixture may have added some loss not accounted for in the model, which requires the modeled wire's diameter to be smaller or length to be longer than that of the actual wire. Nevertheless, the model did reproduce our measurements reasonably well, so we used the model to estimate the two-port scattering-parameters S_{xy}^{F} of the test fixture.

IV. Cable-Assembly and Test-Fixture De-Embedding

We determined the actual (frequency-domain) voltage V_{50} that the photodiode would deliver to an ideal 50-Ω load with small-signal excitation using the voltage V_c measured by our calibrated oscilloscope and our frequency-domain fixture model and cable assembly measurements. Fig. 7 shows a simplified equivalent circuit for the measurement system and illustrates the various reference planes we used to define the measured and calculated scattering parameters.

We determined the reflection coefficient Γ_{p} of the photodiode from the measured reflection coefficient Γ_{m} of the diode mounted in a test fixture using the relation [10], [11]

$$\Gamma_{\mathrm{p}} = \frac{(\Gamma_{\mathrm{m}} - S_{11}^{\mathrm{F}})}{S_{22}^{\mathrm{F}}(\Gamma_{\mathrm{m}} - S_{11}^{\mathrm{F}}) + S_{21}^{\mathrm{F}} S_{12}^{\mathrm{F}}} \tag{2}$$

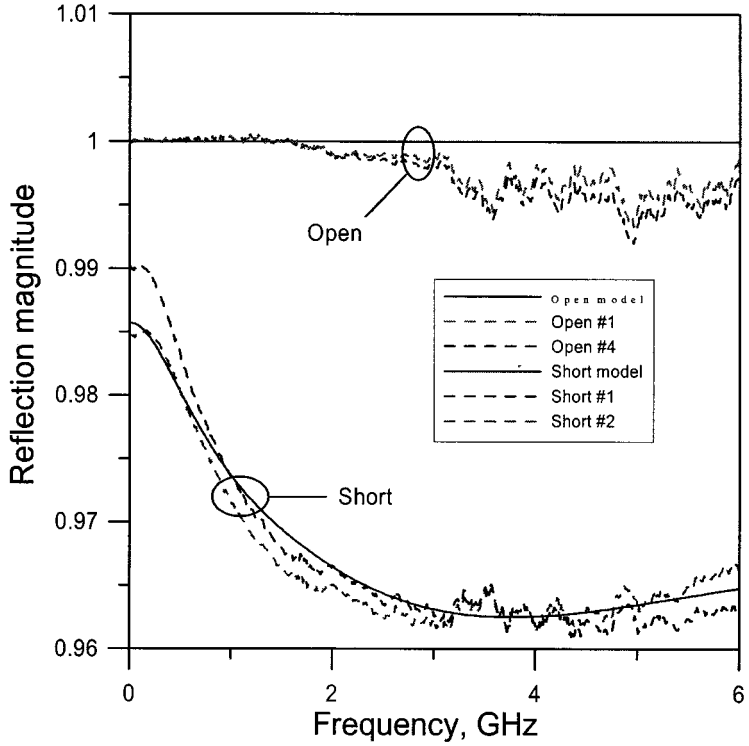

Fig. 5. Measured and modeled reflection coefficient magnitudes of fixture with open and short terminations.

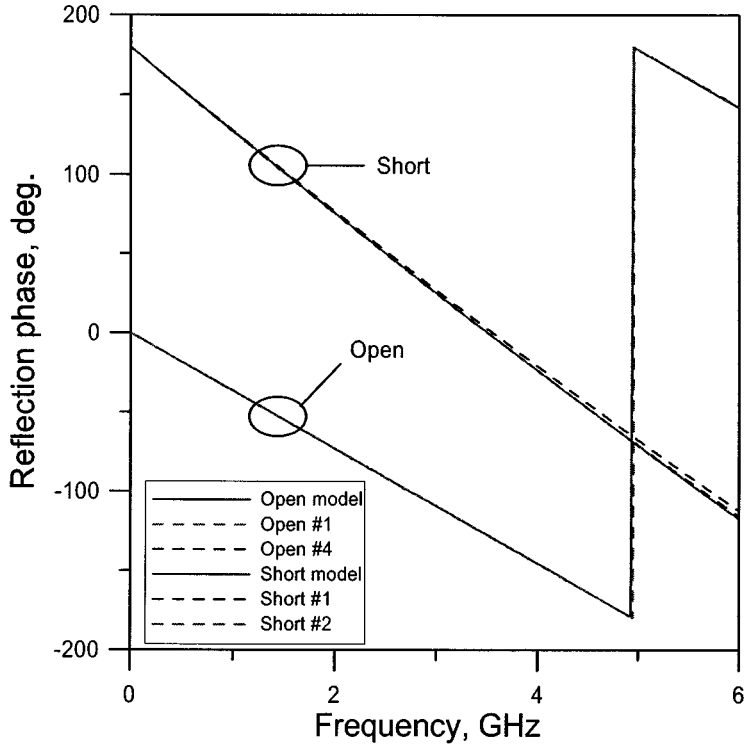

Fig. 6. Measured and modeled reflection coefficient phases of fixture with open and short terminations.

where S_{ij}^{F} represents the two-port scattering parameters of the test fixture. Fig. 8(a) illustrates the equivalent circuit used to define V_{50}, which we found from the relation

$$V_{50} = \frac{V_{\mathrm{c}}}{r_{\mathrm{sp}}} \tag{3}$$

where [10], [11]

$$r_{\mathrm{sp}} = \frac{S'_{21}}{1 - S'_{11}\Gamma_{\mathrm{p}} - S'_{22}\Gamma_{\mathrm{s}} - \Gamma_{\mathrm{s}}\Gamma_{\mathrm{p}}(S'_{21}S'_{12} - S'_{11}S'_{22})}. \tag{4}$$

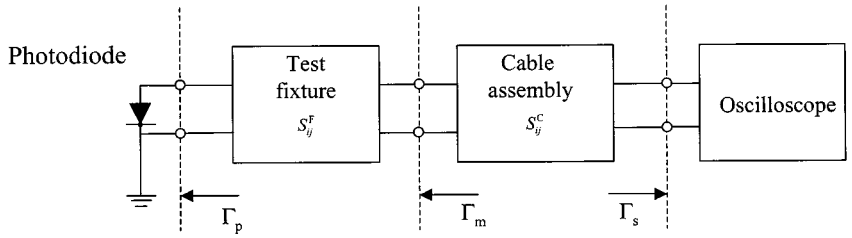

Fig. 7. Simplified circuit model of the photodiode, test fixture, cable assembly, and oscilloscope used for de-embedding unwanted effects.

Here S' is the scattering parameter matrix corresponding to the cascade of the scattering parameters S_{ij}^{F} of the fixture and the scattering parameters S_{ij}^{C} of the cable assembly, which we calculated with the formulae of [10] and [11]. That is, S' is the scattering-parameter matrix of the fixture combined with the cable assembly. Γ_{s} is the reflection coefficient of the oscilloscope. The frequency-domain correction r_{sp} is dimensionless and describes how transmission through and multiple reflections between the fixture and cable assembly modify the wave generated by the photodiode.

V. Norton-Equivalent Current and Thévenin-Equivalent Voltage

We also determined the photodiode's Norton-equivalent current i_{N}, the small-signal current the photodiode delivers to a short circuit, and its Thévenin-equivalent voltage V_{T}, the small-signal voltage it generates across an open circuit. Fig. 8(b) and (c) show the equivalent circuits used in defining the Norton-equivalent current and Thévenin-equivalent voltage. We found the photodiode's Thévenin-equivalent voltage by solving for V_{T} in terms of V_{50}

$$V_{\mathrm{T}} = V_{50} \cdot \frac{Z_{\mathrm{p}} + Z_{\mathrm{r}}}{Z_{\mathrm{r}}} \tag{5}$$

where the photodiode's source impedance Z_{p} is

$$Z_{\mathrm{p}} = Z_{\mathrm{r}} \cdot \frac{1+\Gamma_{\mathrm{p}}}{1-\Gamma_{\mathrm{p}}} \tag{6}$$

and $Z_{\mathrm{r}} = 50\ \Omega$. We found the photodiode's Norton-equivalent current by solving for the current in Fig. 8(c) as

$$i_{\mathrm{N}} = \frac{V_{\mathrm{T}}}{Z_{\mathrm{p}}} = \frac{V_{50}}{Z_{\mathrm{r}}} \cdot \frac{Z_{\mathrm{p}} + Z_{\mathrm{r}}}{Z_{\mathrm{p}}}. \tag{7}$$

VI. Corrected Frequency Response

The dashed curve in Fig. 3 shows the photodiode's frequency response V_{50} determined from (3). This is the magnitude of the voltage that the photodiode would deliver to an ideal 50-Ω load. The response is presented from 0.1 to 6 GHz, over the same region where we believe the fixture model to be valid. The response curve is normalized to 0 dB at 0.1 GHz, which is the lowest frequency point at which we are able to correct the data. The detector's electrical bandwidth (the frequency where the normalized electrical power is -3 dB) is 1.4 GHz.

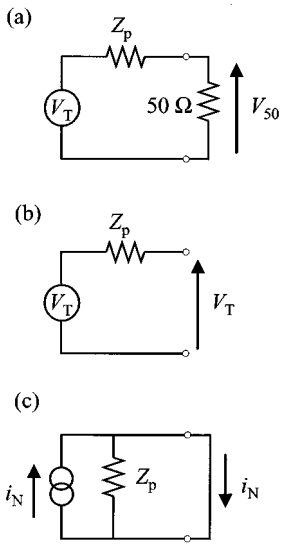

Fig. 8. (a) Circuits used to calculate the voltage delivered to an ideal 50-Ω load. (b) the Thévenin-equivalent voltage V_{T}. (c) Norton-equivalent current, i_{N}.

Fig. 9 compares the corrected frequency response of the voltage V_{50} delivered to a 50-Ω load (dashed line), to that of the Thévenin-equivalent voltage V_{T} (dash/dot line) and the Norton-equivalent current i_{N} (solid line) as defined in (5) and (7): all of the responses are normalized to 0 dB at 100 MHz. The Thévenin-equivalent voltage rises rapidly at the low frequencies and falls off faster than V_{50} at high frequencies. Combining (6) and (7) to give

$$V_{\mathrm{T}} = V_{50} \frac{2}{1-\Gamma_{\mathrm{p}}} \tag{8}$$

shows that, at low frequencies, where the reflection coefficient of the photodiode approaches 1, V_{T} approaches infinity. In practice, V_{T} gets very large at low frequencies, but must be kept much smaller than the bias voltage to maintain our small-signal assumption. V_{T} is also sensitive to small errors in the measurement of Γ_{p}, and, thus, is usually not a convenient measure of photodiode performance.

The Norton-equivalent current is well behaved at the lower frequencies since it reduces to

$$i_{\mathrm{N}} = \frac{V_{50}}{Z_{\mathrm{r}}} \cdot \frac{2}{1+\Gamma_{\mathrm{p}}} \tag{9}$$

and is not singular for $\Gamma_{\mathrm{p}} \to 1$. This is why reverse-biased photodiodes are usually considered current sources. The voltage V_{50}

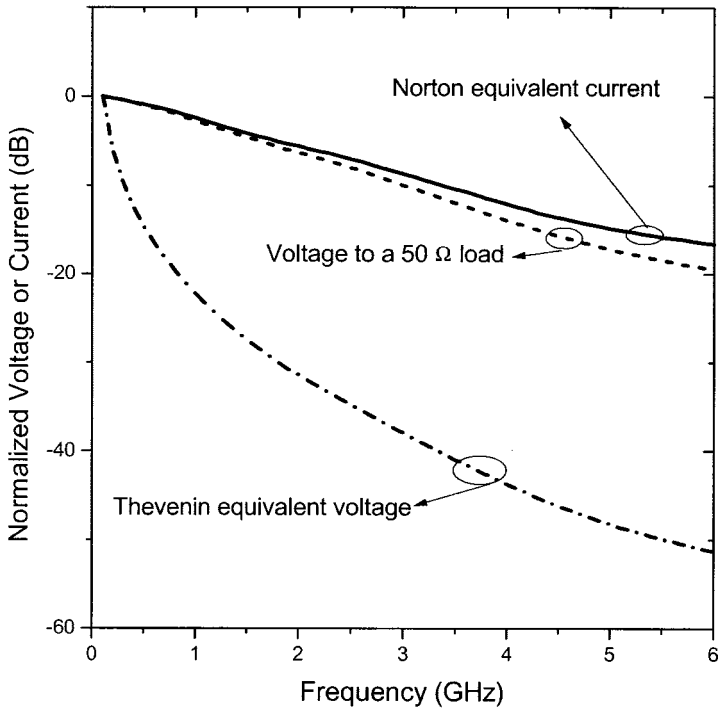

Fig. 9. Corrected frequency response of the voltage V_{50} delivered to a 50-Ω load (dashed line), the Thévenin-equivalent voltage $V_{\rm T}$ (dash/dot line), and the Norton-equivalent current $i_{\rm N}$ (solid line). All responses are normalized to 0 dB at 100 MHz.

delivered to a 50-Ω load is very similar to the Norton-equivalent current because the 50-Ω load is much smaller than the source impedance of the photodiode.

VII. Conclusion

We developed a rigorous calibration and measurement procedure that determines the frequency response of gigabit chip photodiodes embedded in simple test fixtures. Our particular fixture had a useful frequency range limited to about 6 GHz and would have benefited from using a connector and fixture designed for high-frequency operation. We characterized and accounted for mismatch and loss in the bias T, adapters, cables, and test fixture, and for nonidealities in the oscilloscope. This allowed us to fully calibrate the measurements and to directly determine intrinsic electrical parameters describing the photodiode in the frequency domain. Our method for applying frequency-domain corrections to time-domain measured data is also applicable to other measurements over the entire 50-GHz bandwidth of the oscilloscope when the electrical properties of the test fixture and photodiode can be fully characterized up to 50 GHz.

References

[1] J. Verspecht and K. Rush, "Individual characterization of broadband sampling oscilloscopes with a nose-to-nose calibration procedure," *IEEE Trans. Instrum. Meas.*, vol. 43, pp. 347–354, Apr. 1994.

[2] J. Verspecht, "Broadband sampling oscilloscope characterization with the 'nose-to-nose' calibration procedure: A theoretical and practical analysis," *IEEE Trans. Instrum. Meas.*, vol. 44, pp. 991–997, Dec. 1995.

[3] ——, "Calibration of a measurement system for high frequency nonlinear devices," Ph.D. dissertation, Free University of Brussels, Brussels, Belgium, Sept. 1995.

[4] P. D. Hale, T. S. Clement, K. J. Coakley, C. M. Wang, D. C. DeGroot, and A. P. Verdoni, "Estimating the magnitude and phase response of a 50 GHz sampling oscilloscope using the 'nose-to-nose' method," in *55th ARFTG Conf. Dig.*, June 2000, pp. 35–42.

[5] C. M. Wang, P. D. Hale, and K. J. Coakley, "Least-squares estimation of time-base distortion of sampling oscilloscopes," *IEEE Trans. Instrum. Meas.*, vol. 48, pp. 1324–1332, 1999.

[6] D. C. DeGroot, P. D. Hale, M. Vanden Bosche, F. Verbeyst, and J. Verspecht, "Analysis of interconnection networks and mismatch in the nose-to-nose calibration," in *55th ARFTG Conf. Dig.*, June 2000, pp. 116–121.

[7] K. J. Coakley and P. D. Hale, "Alignment of noisy signals," *IEEE Trans. Instrum. Meas.*, vol. 50, pp. 141–149, 2001.

[8] T. S. Clement, P. D. Hale, K. C. Coakley, and C. M. Wang, "Time-domain measurement of the frequency response of high-speed photoreceivers to 50 GHz," in *Tech. Dig. Symp. Optical Fiber Measurement*, 2000, Nat. Inst. Std. Technol. SP 953, pp. 121–124.

[9] S. Ramo, J. R. Whinnery, and T. Van Duzer, Eds., *Fields and Waves in Communications Electronics*, 2nd ed. New York: Wiley, 1965, pp. 178–183.

[10] D. M. Kerns and R. W. Beatty, *Basic Theory of Waveguide Junctions and Introductory Microwave Network Analysis*. Oxford, U.K.: Pergamon, 1967, pp. 42–43, 72–83, 121.

[11] "S-parameter design," Hewlett Packard application note 154, Apr. 1972.

Paul D. Hale (M'01) received the Ph.D. degree in applied physics from the Colorado School of Mines, Golden, CO, in 1985 and 1989.

He has been a Staff Member of the National Institute of Standards and Technology (NIST), Boulder, CO, since 1989 and has conducted research in birefringent devices, mode-locked fiber lasers, fiber chromatic dispersion, broadband lasers, interferometry, polarization standards, and high-speed optoelectronic measurements. He is presently Leader of the High-Speed Measurements Project in the Sources and Detectors Group. His research interests include high-speed optoelectronic and microwave measurements and their calibration. He is currently an Associate Editor of the JOURNAL OF LIGHTWAVE TECHNOLOGY.

Dr. Hale, along with a team of four scientists, received the Department of Commerce Gold Medal in 1994 for measuring fiber cladding diameter with an uncertainty of 30 nm. In 1998, he received a Department of Commerce Bronze Medal, along with four other scientists, for developing measurement techniques and standards to determine optical polarization parameters.

Tracy S. Clement (S'89–M'92) received the Ph.D. degree in electrical engineering from Rice University, Houston, TX, in 1993. Her Ph.D. research involved developing and studying short wavelength (XUV and VUV) lasers and ultrashort pulse laser systems.

She has been with the Optoelectronics Division of the National Institute of Standards and Technology (NIST), Boulder, CO, since 1998. Prior to joining the Optoelectronics Division, she was with JILA, the Quantum Physics Department of NIST, and she was an Assistant Professor Adjoint in the Department of Physics at the University of Colorado, Boulder. From 1993 to 1995, she was a Director's Postdoctoral Fellow at Los Alamos National Laboratory, Los Alamos, NM. Her research interests include measuring response of high-speed electrooptic components and ultrashort pulse laser measurements.

Dylan F. Williams (S'82–M'86–SM'90) received the Ph.D. degree in electrical engineering from the University of California, Berkeley, in 1986.

In 1989, he joined the Electromagnetic Fields Division of the National Institute of Standards and Technology, Boulder, CO, where he develops metrology for characterization of monolithic microwave integrated circuits and electronic interconnects. He has published more than 80 technical papers.

Dr. Williams has received the Department of Commerce Silver and Bronze Medals, the Electrical Engineering Laboratory's Outstanding Paper Award, two ARFTG Best Paper Awards, the ARFTG Automated Measurements Technology Award, and the IEEE Morris E. Leeds Award.

Elyas Balta received the B.S. degree in applied physics from California State University, Dominguez Hills, in 1998.

He was formerly with United Detectors Technology, Inc., Hawthorne, CA, where he was the Optical Metrology Laboratory Supervisor in charge of research and development experiments for a wide variety of light detection applications and setting electrooptical standards throughout the company and its subsidiaries. He headed the testing efforts of high-speed photodiodes for use in the telecommunications industry for up to Sonet OC-48. In July 2000, he moved to Integrated Micromachines, Inc., Monrovia, CA, a telecommunications startup where he is currently the Product Test Manager. He is in charge of all of the optical test design and execution of attenuator switches and the high port count all-optical switch targeted toward the fiber-optic industry.

Narayan D. Taneja, photograph and biography not available at the time of publication.